Rational Design of Polymers for Selective CO_2 Reduction Catalysis

Jane J. Leung,[†] Julian A. Vigil,[†] Julien Warnan,[†] Esther Edwardes Moore and Erwin Reisner[*]

Abstract: A series of copolymers comprising a terpyridine ligand and various functional groups were synthesized toward integrating a Co-based molecular CO_2 reduction catalyst. Using porous metal oxide electrodes designed to host macromolecules, the Co-coordinated polymers were readily immobilized *via* phosphonate anchoring moieties. Within the polymeric matrix, the outer coordination sphere of the Co terpyridine catalyst was engineered using hydrophobic functional moieties to improve CO_2 reduction selectivity in the presence of water. Electrochemical and photoelectrochemical CO_2 reduction were demonstrated with the polymer-immobilized hybrid cathodes, with a CO:H_2 product ratio of up to 6:1 compared to 2:1 for a corresponding "monomeric" Co terpyridine catalyst. This versatile platform of polymer design demonstrates promise in controlling the outer-sphere environment of synthetic molecular catalysts, analogous to CO_2 reductases.

Electrocatalytic reduction of CO_2 selectively to CO remains a major goal toward realizing a sustainable, closed carbon cycle.[1] To this end, molecular catalysts have been developed taking inspiration from natural archetypes such as CO and formate dehydrogenase enzymes.[2] While still dominated by precious metal-based complexes, tremendous efforts have recently been focused on designing Earth-abundant 3d transition metal-based catalysts.[3] Often limited by their low stability and solubility, as well as the low concentration of CO_2 and competing H_2 evolution in water, examples of first row transition metals performing aqueous CO_2 reduction remain scarce.

Since early reports of Ni cyclam[4] and Lehn's Re[5] catalysts, optimizing molecular design toward improved product selectivity has principally involved tailoring the metal's primary coordination sphere.[3] Alternative strategies have incorporated catalysts almost exclusively with carbon materials to provide hybrid electrodes with a hydrophobic environment conducive to CO_2 utilization, even in water.[6] Considering their facile preparation and stability in water, metal oxides represent an alternative class of promising materials, and have been successfully exploited both in photocatalytic colloidal schemes and as cathode substrates toward H_2 evolution.[7] However, their hydrophilicity and propensity toward hydrogen bonding generally promote H_2 evolution over CO_2 reduction.

Here, we report the development of the first rationally designed polymers for selective CO production and their incorporation into porous electrode architectures to produce precious metal-free CO_2 reduction cathodes. Building upon our recent utilization of a phosphonated Co bis(tpy) catalyst (tpy = 2,2':6',2"-terpyridine), **CotpyP** (see Supporting Information), toward photoelectrochemical reduction of CO_2 in aqueous environments,[8] we demonstrate that integrating the CO_2 reduction catalyst in a rationally designed copolymer is a promising strategy for engineering the outer-sphere environment around the metal center to achieve improved CO_2 reduction performance.[2a, 9]

Copolymer scaffolds were synthesized with three monomers (Fig. 1a): a tpy ligand; a phosphonic acid anchoring moiety; and a variable functional group. Free-radical polymerization of the synthesized methacrylate-bearing tpy (**1**) and diethyl phosphonate (**2**) monomers in stoichiometric combination with either a methyl or n-decyl methacrylate (**3** and **4**, respectively) monomer produced the tpy-phosphonate ester copolymers (**5**, **6**). The phosphonate ester moieties of the latter were deprotected to yield the final low molecular weight copolymer scaffolds **p1** and **p2** (M_n = 3.2 and 3.1 kDa, respectively). All synthetic procedures and characterization details are provided in the Supporting Information.

Addition of $Co(BF_4)_2$ to a solution of **p1** yields **P1$_x$** (x represents the number of Co equivalents per two tpy units in the polymer; Fig. 1a). The coordinated polymers are depicted schematically in Fig. 1b, showing the role of the polymer backbone and functionalities near the active Cotpy complexes, and an interplay between Co loading/coordination and crosslinking of polymer chains. Cyclic voltammetry (CV) of dissolved **P1$_1$** (1:2 Co:tpy ratio) in a 95:5 (v:v) DMF:H_2O solution using a glassy carbon working electrode with tetrabutylammonium tetrafluoroborate ($TBABF_4$, 0.1 M) under N_2 atmosphere shows reversible electrochemical features between 0.0 and –2.0 V *vs* $Fc^{+/0}$ (Fig. S1a). Square wave voltammetry (SWV) affords better resolution due to improved Faradaic-to-capacitive current ratios (Fig. S1b).

The most positive waves [$E_{1/2}$ = –0.46 (C_1), –0.56 (C_2) V *vs* $Fc^{+/0}$] are attributed to the $Co^{III/II}$ couple of the Co bis(tpy) complex, followed by two waves [$E_{1/2}$ = –1.52 (C_3), –1.63 (C_4) V *vs* $Fc^{+/0}$] assigned to $Co^{II/I}$ couples (Fig. S1b).[10] We assigned the discrete features C_1-C_4 of the Co-based redox processes (also observed for the immobilized polymers, see below) to the differences in preferential polymer folding configurations and/or solvation in mixed solvents that generate varying chemical environments. We attribute the wave at −1.8 V *vs* $Fc^{+/0}$ (C_5) to the $Co^{II/I}$ couple of the "unmated" Co mono(tpy) complex - in accordance with previous publications - as a result of the polymeric matrix.[9b, 11] Finally, a coordinated tpy-based reduction is observed below –2.3 V *vs* $Fc^{+/0}$ (C_6), which corresponds with the onset of current enhancement in the presence of CO_2 (Fig. S1a).[10a]

J. J. Leung[†], J. A. Vigil[†], Dr. J. Warnan[†], E. Edwardes Moore, Prof. E. Reisner
Christian Doppler Laboratory for Sustainable SynGas Chemistry, Department of Chemistry, University of Cambridge, Cambridge CB2 1EW, United Kingdom
Homepage: http://www-reisner.ch.cam.ac.uk

[†] These authors contributed equally to this work.
[*] Corresponding author e-mail: reisner@ch.cam.ac.uk

Supporting information for this article is given via a link at the end of the document.

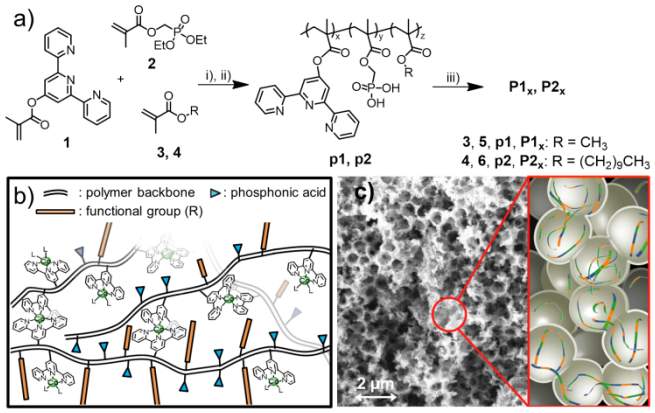

Figure 1. a) Synthetic route to the **P1x** and **P2x** polymers: i) 2,2′-azobis(2-methylpropionitrile), THF, 70 °C, 16 h; ii) (1) bromotrimethylsilane, DCM, 0 °C, 16 h, (2) MeOH, 4 h; iii) $Co(BF_4)_2{\cdot}6H_2O$, MeOH, 16 h. b) Schematic representation of **P1x** and **P2x**. c) Scanning electron microscope image of IO-TiO_2 and schematic representation of polymer chains embedded in the porous scaffold.

The interplay between Co loading and coordination was investigated using ultraviolet-visible (UV-Vis) spectroscopy for **p1** and a series of coordinated **P1x** polymers (Fig. 2a). Upon the addition of Co^{2+} to **p1** in 0.6 or 1 equiv to every two tpy units (**P1$_{0.6}$** or **P1$_1$**, respectively), three absorption maxima are observed at 440, 505 and 550 nm, attributed to Co(II) bis(tpy) metal-to-ligand charge transfer transitions.[12] At concentrations of Co corresponding to mono(tpy) stoichiometry (**P1$_2$**) and a further excess of Co (**P1$_5$**), the spectra show concomitant loss of the Co(II) bis(tpy) transitions and emergence of a broad absorption in the UV region around 380 nm, characteristic of the Co(II) mono(tpy) complex (Fig. 2a, inset).[13] This dynamic coordination equilibrium within the polymeric matrix – primarily bis(tpy) coordination in **P1$_{0.6/1}$** converting into mono(tpy) coordination in **P1$_{2/5}$** – is likely accompanied by a reduction in the degree of crosslinking.

The **P1x** polymers were readily immobilized on fluorine-doped tin oxide-supported inverse opal indium tin oxide electrodes (FTO|IO-ITO; 6 µm film thickness, IO pore Ø = 750 nm, ITO particle size < 50 nm, geometrical surface area (*S*) = 0.28 cm^2) by immersion in various **P1x** sensitizing solutions ([Co^{2+}] = 0.25 mM and [tpy] = 0.92, 0.55, 0.28 or 0.11 mM). The IO-ITO electrodes were previously optimized to host proteins,[14] and are used here to accommodate a high loading of the polymers within the 3D architecture.

The immobilized **P1x** polymers were initially characterized using sequential electrochemical techniques in dry DMF electrolyte solution. Following an initial SWV scan, the electrode was cycled 20 times by CV to monitor changes in the coordination environment of Co. The FTO|IO-ITO|**P1$_1$** electrode shows two stable, reversible waves corresponding to the $Co^{II/II}$ and $Co^{II/I}$ couples ($E_{1/2}$ = –0.10 and –1.15 V *vs* $Fc^{+/0}$; Fig. 2b, left) of the Co bis(tpy) complex.[10] In contrast, the initial SWV scan for the FTO|IO-ITO|**P1$_2$** electrode shows two primary features at –0.85 and –1.35 V *vs* $Fc^{+/0}$ attributed to the Co mono(tpy) complex,[15] which subsequently decay with cycling (Fig. 2b, right). The final SWV scan indicates complete loss of these features and the emergence of Co bis(tpy) features, suggesting that the more thermodynamically stable Co bis(tpy) complex is formed with cycling, accompanied by a loss of excess Co ions. The redox behavior and stability of the immobilized **P1$_{0.6}$** and **P1$_5$** polymers were analogous to **P1$_1$** and **P1$_2$**, respectively, in both dry DMF (Fig. S2) and in the presence of 5% H_2O (Fig. S3). In general, decreasing peak currents in these voltammograms when progressing from **P1$_{0.6}$** to **P1$_5$** may be attributed to lower loadings of the corresponding polymers as a result of the sensitizing solution concentration (see above).

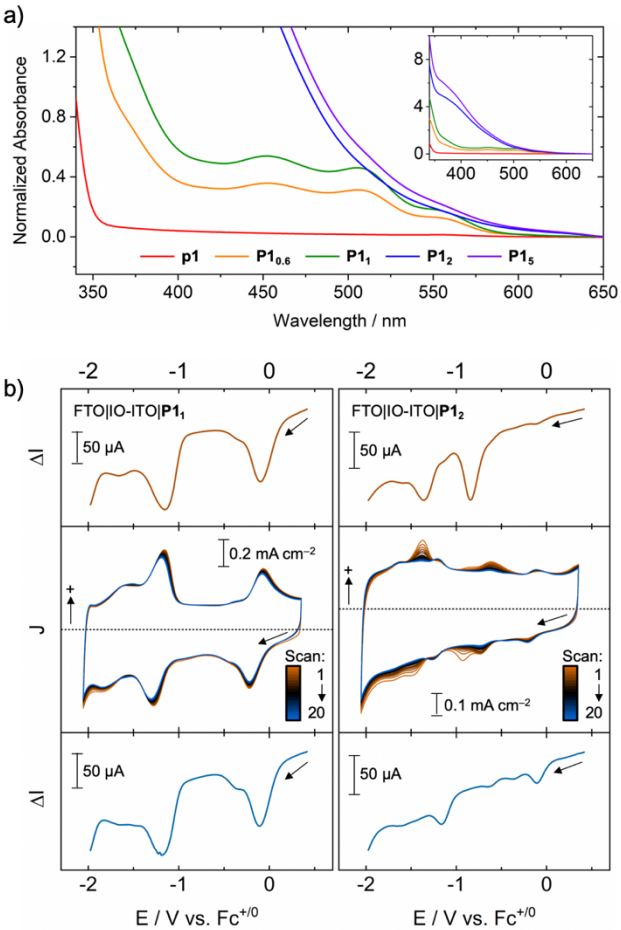

Figure 2. a) UV-Vis spectra of **p1** (0.5 mM tpy) and the Co-coordinated **P1x** polymers in MeOH (0.25 mM Co) (normalized to [tpy]). b) Sequential electroanalytical characterization of the immobilized **P1$_1$** (left) and **P1$_2$** (right) polymers on FTO|IO-ITO electrodes: initial SWV (top), followed by 20 CV cycles (middle) and a final SWV (bottom); dry DMF (0.1 M $TBABF_4$), N_2-purged, 100 mV s^{-1}, room temperature (RT). Arrows indicate scan starts, dashed lines indicate J = 0 mA cm^{-2}.

The **P1x** polymers were subsequently immobilized on Ti foil-backed inverse opal TiO_2 electrodes (Ti|IO-TiO_2; 15 µm film thickness, IO pore Ø = 750 nm, TiO_2 anatase particle size 10-30 nm, *S* = 0.28 cm^2; Fig. 1c and S4) for evaluation of their electrocatalytic CO_2 reduction activity by controlled potential electrolysis (CPE). Ti|IO-TiO_2 was chosen over FTO|IO-ITO owing to its greater stability paired with suitable conductivity under reducing conditions. The quantity of Co loaded per geometric surface area, measured by inductively coupled plasma optical emission spectrometry (ICP-OES), increased

approximately proportionately with the Co:tpy ratio in the immobilized polymers (Table S1). Attenuated total reflectance Fourier transform infrared (ATR-FTIR) spectroscopy confirmed the integrity of the polymers upon immobilization (Fig. S5).

CPE was carried out at an applied potential (E_{app}) of –1.3 V *vs* $Fc^{+/0}$ in a CO_2-saturated 6:4 (v:v) MeCN:H_2O electrolyte solution (0.1 M $TBABF_4$). This electrolyte composition was previously optimized for the analogous molecular **CotpyP** catalyst immobilized on porous TiO_2 electrodes,[8] and the catalytic onset from the FTO|IO-ITO|**P1$_1$** electrode was observed at potentials close to –1.3 V *vs* $Fc^{+/0}$ in the presence of CO_2 (Fig. S6). Electrocatalysis is observed at potentials 0.7 V more positive compared to that in solution, which is in accordance with our previous observations of **CotpyP** immobilized on TiO_2 electrodes.[8]

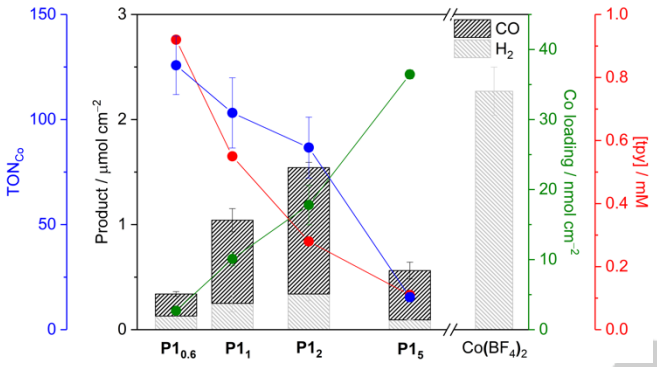

Figure 3. CPE of Ti|IO-TiO_2|**P1$_x$** electrodes after 4 h: product distribution, TON_{Co}, Co surface loading (as determined by ICP-OES) and tpy concentration (as determined by the known concentration of the tpy co-monomer in the **P1$_x$** immobilization solution). The x-axis is presented on a $\log_{10}$ scale according to x (**P1$_x$**). Product distribution from CPE of Ti|IO-TiO_2|Co(BF_4)$_2$ is included for comparison. Conditions: 6:4 MeCN:H_2O (0.1 M $TBABF_4$), CO_2-purged, E_{app} = −1.3 V *vs* $Fc^{+/0}$, RT.

While the stability of each electrode was similar regardless of Co loading (Fig. S7), striking differences in overall activity and Co-based turnover numbers (TON_{Co}s) were observed for the production of H_2 and CO (Fig. 3 and Table S2). After 4 h of CPE, the total amount of product increased from 0.34 μmol cm^{-2} for Ti|IO-TiO_2|**P1$_{0.6}$** to 1.54 μmol cm^{-2} for Ti|IO-TiO_2|**P1$_2$**. Increasing the Co loading further (Ti|IO-TiO_2|**P1$_5$**) led to a decrease in activity, with only 0.56 μmol cm^{-2} of product. Accounting for the variation in Co loading on these electrodes (Table S1), the maximum total TON_{Co} (126, of which 78 is CO) was observed for the polymer with the lowest Co loading, Ti|IO-TiO_2|**P1$_{0.6}$**, and the other electrodes yielded progressively lower total TON_{Co}s with increasing Co loading (Table S2).

Considering the aforementioned coordination equilibrium in the polymeric matrix, we observe that the greatest TON_{Co} can be achieved when Co is primarily in a bis(tpy) coordination environment (Fig. 3 and Table S2). Thus, in the case of **P1$_1$** and **P1$_2$**, a mixture of mono(tpy) and bis(tpy) environments results in a trade-off between overall product evolution [1.54 μmol cm^{-2} (Ti|IO-TiO_2|**P1$_2$**) > 1.04 μmol cm^{-2} (Ti|IO-TiO_2|**P1$_1$**)] and TON [87 (Ti|IO-TiO_2|**P1$_2$**) < 103 (Ti|IO-TiO_2|**P1$_1$**)] after 4 h.[8] The low activity of the Ti|IO-TiO_2|**P1$_5$** electrode is attributed to a minimal amount of Co bis(tpy) complexes that form after initial leaching of excess Co ions from the electrode.

To quantify the loss of Co under catalytic conditions, the Co loading was determined by ICP-OES for FTO|IO-ITO|**P1$_5$** before and after cycling to –1.3 V *vs* $Fc^{+/0}$ in the electrolyte solution. After 20 cycles, the Co loading on the electrode decreased by 75% relative to the electrode before cycling (Table S3). Finally, the inactivity of excess (uncoordinated) Co ions toward CO_2 reduction was confirmed by CPE of a Ti|TiO_2 electrode soaked in a Co(BF_4)$_2$ solution (57±1 nmol cm^{-2} Co; Fig. 3). Modest Faradaic efficiencies (FEs) recorded for the Ti|IO-TiO_2|**P1$_x$** electrodes (Table S2) may be attributed to fundamental limitations of the Co bis(tpy) complex,[15a] unproductive charge transfer pathways along the polymer backbone, as well as capacitive currents from TiO_2 and reduction of trapped O_2 within the mesoporous network, alongside entrapment of products within the highly porous inverse opal architecture.[16]

Additional control CPE experiments confirmed that both CO_2 and H^+ reduction are carried out exclusively by the **P1$_x$** polymers (Fig. S7-S8), and that CO_2 is the source of CO (Fig. S9-S10). The stable activity of these electrodes (Fig. S7) and ATR-FTIR measurements taken after CPE (Fig. S5) both indicate preserved integrity of the **P1$_x$** polymers under catalytic conditions.

Thus, modulating the Co loading and thereby the distribution of Co coordination environments within the polymeric matrix has allowed tuning and optimizing of the electrocatalytic CO_2 reduction activity. To take further advantage of the versatile synthetic platform, **3** was replaced by a more hydrophobic monomer, **4**, in order to decrease the hydrophilicity in the vicinity of the catalyst and inhibit H^+ reduction (Fig. 1). Coordination of **p2** with Co(II) in bis(tpy) stoichiometry yields **P2$_1$**, the redox behavior of which was synonymous to **P1$_1$** both in solution (Fig. S11) and immobilized on FTO|IO-ITO electrodes (Fig. S12).

Table 1. CPE results from Ti|IO-TiO_2|**P1$_1$** and Ti|IO-TiO_2|**P2$_1$** electrodes after 4 h. Conditions: 6:4 MeCN:H_2O (0.1 M $TBABF_4$), CO_2-purged, E_{app} = −1.3 V *vs* $Fc^{+/0}$, RT.

Polymer	Product (μmol cm^{-2})		TON_{Co}		Selectivity (CO/H_2)
	CO	H_2	CO	H_2	
P1$_1$	0.79±0.11	0.25±0.08	78±13	25±8	3.2±1.1
	Combined = 1.04±0.14		Combined = 103±17		
P2$_1$	0.97±0.11	0.18±0.03	98±11	18±4	5.3±1.2
	Combined = 1.15±0.12		Combined = 116±12		

Upon immobilization of **P2$_1$** on Ti|IO-TiO_2 electrodes, the CO_2 reduction activity of the resulting Ti|IO-TiO_2|**P2$_1$** cathodes revealed a distinct difference in the product selectivity compared to **P1$_1$** (Table 1; Fig. S13 and S14; Co loading on Ti|IO-TiO_2|**P2$_1$** was within error of that for Ti|IO-TiO_2|**P1$_1$**, Table S1). While the combined product yields and TON_{Co}s for CO and H_2 production were similar between the two polymers after 4 h of CPE, Ti|IO-TiO_2|**P2$_1$** produced more CO and less H_2 than Ti|IO-TiO_2|**P1$_1$**, leading to a CO/H_2 ratio of 5.3 for the former compared to 3.2 for the latter. The difference is greater at t = 2 h, when this ratio reaches 6.0 for Ti|IO-TiO_2|**P2$_1$**, corresponding to 86% selectivity

for CO. Control experiments under N_2 (Fig. S15) and isotopic labelling experiments (Fig. S16) confirmed CO_2 as the origin of CO. ATR-FTIR does not suggest modification or degradation of **P2$_1$**, both upon immobilization and after CPE (Fig. S17).

The product selectivity of **P2$_1$** is also a significant improvement relative to that of the molecular **CotpyP** catalyst, which produces CO at 69% selectivity (CO/H_2 = 2.3) on the same electrode (Fig. S18). This highlights the possibility of improving selectivity by modification to the outer coordination sphere of a molecular catalyst rather than the catalyst's primary ligand structure.[9a, 9b] The relatively low turnover frequencies of **P2$_1$**-based electrodes (~0.007 s^{-1}) compares well with those of **CotpyP**-based electrodes (~0.009 s^{-1}), suggesting that the polymeric scaffold does not impede catalysis. Similar kinetic limitations were previously observed for other Co bis(terpyridine) catalysts immobilized on electrodes in aqueous and MeCN electrolysis conditions,[11b, 17] which could originate from the anchored catalyst's reduced degrees of freedom or, in this case, from the limited diffusion of CO_2 within the porous electrodes.

As the most selective polymer toward CO production, **P2$_1$** was immobilized on a *p*-type Si (Si) semiconductor electrode for photoelectrochemical CO_2 reduction. This was enabled by interfacing a compatible IO-TiO_2 layer with light-harvesting Si as previously reported.[18]

Linear sweep voltammograms under chopped illumination were conducted on the Si|IO-TiO_2|**P2$_1$** photocathode in the same electrolyte solution as that used for the Ti|IO-TiO_2|**P2$_1$** cathodes (Fig. S19a). A photocurrent onset at −0.5 V *vs* $Fc^{+/0}$ and density of −450 μA cm^{-2} at −1.0 V *vs* $Fc^{+/0}$ were observed, which compares favorably to the −150 μA cm^{-2} achieved by a polymer-free Si|IO-TiO_2 control electrode.[18] Controlled potential photoelectrolysis at −1.0 V *vs* $Fc^{+/0}$ under irradiation (100 mW cm^{-2}, AM1.5G, λ > 400 nm) on the Si|IO-TiO_2|**P2$_1$** electrode produced CO at ~80% product selectivity over 6 h (Fig. S19b-c). The low FE is coherent with the electrocatalysis results and highlights the need for a more inert or conductive polymer backbone and/or more efficient electron transfer between the surface and the polymer. Neither the catalyst-free Si|IO-TiO_2 photoelectrode under CO_2 nor Si|IO-TiO_2|**P2$_1$** under N_2 produced detectable amounts of CO or H_2 (Fig. S19b).

In conclusion, rationally designed coordination polymers have been demonstrated as a versatile platform to achieve tunable molecular CO_2 reduction catalysis in the presence of water. By first modulating the degree of crosslinking *via* Co loading in the polymer matrix, an equilibrium between mono(tpy) and bis(tpy) complexes was established that ultimately favors the more stable bis(tpy) complex and therefore electrocatalytic CO evolution. Next, the choice of functional group monomer was aimed toward the provision of an artificially engineered environment for the active Co bis(tpy) complex to improve selective CO production. This was demonstrated by the improvement of the $CO:H_2$ product ratio from 2:1 (for the analogous molecular catalyst) to 6:1 for the polymer containing a hydrophobic alkyl chain conducive to CO_2 utilization. The synergy of the polymer functionality with porous IO electrode architectures was further demonstrated on Si|IO-TiO_2 photoelectrodes, where selective solar-driven CO_2 reduction was achieved. The strategy presented here motivates further development of catalyst-containing polymers with tailored functionality toward catalytic activity, selectivity and stability.

Acknowledgements

This work was supported by the Woolf Fisher Trust in New Zealand (J. J. L.), the Winston Churchill Foundation of the United States (J. A. V.), the Christian Doppler Research Association (Austrian Federal Ministry for Digital and Economic Affairs and the National Foundation for Research, Technology and Development), the OMV Group (J. W., E. E. M., E. R.). We also gratefully acknowledge Dr. Katarzyna P. Sokol, Dr. Dong Heon Nam, Andreas Wagner and Kenichi Nakanishi for providing electrode materials and Daniel Whitaker for help with gel permeation chromatography measurements.

Keywords: polymers • electrochemistry • catalysis • CO_2 reduction • artificial photosynthesis

[1] J. A. Herron, J. Kim, A. A. Upadhye, G. W. Huber, C. T. Maravelias, *Energy Environ. Sci.* **2015**, *8*, 126-157.

[2] a) M. Can, F. A. Armstrong, S. W. Ragsdale, *Chem. Rev.* **2014**, *114*, 4149-4174; b) F. A. Armstrong, J. Hirst, *Proc. Natl. Acad. Sci.* **2011**, *108*, 14049-14054.

[3] K. E. Dalle, J. Warnan, J. J. Leung, B. Reuillard, I. S. R. Karmel, E. Reisner, *Chem. Rev.* **2019**, *119*, 2752-2875.

[4] J. P. Collin, A. Jouaiti, J. P. Sauvage, *Inorg. Chem.* **1988**, *27*, 1986-1990.

[5] J. Hawecker, J.-M. Lehn, R. Ziessel, *J. Chem. Soc., Chem. Commun.* **1984**, 328-330.

[6] a) B. Reuillard, K. H. Ly, T. E. Rosser, M. F. Kuehnel, I. Zebger, E. Reisner, *J. Am. Chem. Soc.* **2017**, *139*, 14425-14435; b) M. Wang, L. Chen, T.-C. Lau, M. Robert, *Angew. Chem. Int. Ed.* **2018**, *57*, 7769-7773.

[7] a) H. Tian, *ChemSusChem* **2015**, *8*, 3746-3759; b) J. Willkomm, K. L. Orchard, A. Reynal, E. Pastor, J. R. Durrant, E. Reisner, *Chem. Soc. Rev.* **2016**, *45*, 9-23.

[8] J. J. Leung, J. Warnan, K. H. Ly, N. Heidary, D. H. Nam, M. F. Kuehnel, E. Reisner, *Nat. Catal.* **2019**, in print (DOI: 10.1038/s41929-019-0254-2).

[9] a) W. W. Kramer, C. C. L. McCrory, *Chem. Sci.* **2016**, *7*, 2506-2515; b) B. Reuillard, J. Warnan, J. J. Leung, D. W. Wakerley, E. Reisner, *Angew. Chem. Int. Ed.* **2016**, *55*, 3952-3957; c) S. Sahu, P. L. Cheung, C. W. Machan, S. A. Chabolla, C. P. Kubiak, N. C. Gianneschi, *Chem. Eur. J.* **2017**, *23*, 8619-8622.

[10] a) N. Elgrishi, M. B. Chambers, V. Artero, M. Fontecave, *Phys. Chem. Chem. Phys.* **2014**, *16*, 13635-13644; b) N. Elgrishi, M. B. Chambers, X. Wang, M. Fontecave, *Chem. Soc. Rev.* **2017**, *46*, 761-796.

[11] a) H. D. Abruña, *Coord. Chem. Rev.* **1988**, *86*, 135-189; b) J. A. Ramos Sende, C. R. Arana, L. Hernandez, K. T. Potts, M. Keshevarz-K, H. D. Abruña, *Inorg. Chem.* **1995**, *34*, 3339-3348.

[12] C. Enachescu, I. Krivokapic, M. Zerara, J. A. Real, N. Amstutz, A. Hauser, *Inorg. Chim. Acta* **2007**, *360*, 3945-3950.

[13] J. S. Judge, W. A. Baker, *Inorg. Chim. Acta* **1967**, *1*, 239-244.

[14] D. Mersch, C.-Y. Lee, J. Z. Zhang, K. Brinkert, J. C. Fontecilla-Camps, A. W. Rutherford, E. Reisner, *J. Am. Chem. Soc.* **2015**, *137*, 8541-8549.

[15] a) N. Elgrishi, M. B. Chambers, M. Fontecave, *Chem. Sci.* **2015**, *6*, 2522-2531; b) N. Elgrishi, S. Griveau, M. B.

Chambers, F. Bedioui, M. Fontecave, *Chem. Commun.* **2015**, *51*, 2995-2998.

[16] a) J. J. Leung, J. Warnan, D. H. Nam, J. Z. Zhang, J. Willkomm, E. Reisner, *Chem. Sci.* **2017**, *8*, 5172-5180; b) K. P. Sokol, W. E. Robinson, A. R. Oliveira, J. Warnan, M. M. Nowaczyk, A. Ruff, I. A. C. Pereira, E. Reisner, *J. Am. Chem. Soc.* **2018**.

[17] H. C. Hurrell, A. L. Mogstad, D. A. Usifer, K. T. Potts, H. D. Abruña, *Inorg. Chem.* **1989**, *28*, 1080-1084.

[18] D. H. Nam, J. Z. Zhang, V. Andrei, N. Kornienko, N. Heidary, A. Wagner, K. Nakanishi, K. P. Sokol, B. Slater, I. Zebger, S. Hofmann, J. C. Fontecilla-Camps, C. B. Park, E. Reisner, *Angew. Chem. Int. Ed.* **2018**, *57*, 10595-10599.

Entry for the Table of Contents

Layout 2:

COMMUNICATION

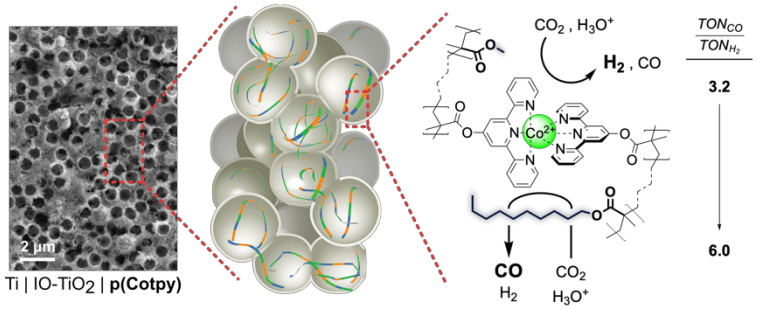

*Jane J. Leung,[†] Julian A. Vigil,[†] Julien Warnan,[†] Esther Edwardes Moore and Erwin Reisner**

Page No. – Page No.

Rational Design of Polymers for Selective CO_2 Reduction Catalysis

A series of copolymers incorporating Co bis(terpyridine) complexes was synthesized and integrated into porous metal oxide electrodes conceived to host macromolecules towards supported CO_2 reduction. The versatile platform of polymer design demonstrates promise in tuning the outer-sphere environment of synthetic molecular catalysts to improve its product selectivity, emulating the strategy found in CO_2 reductases.